A Cavity Activation and Bubble Growth Model of the Leidenfrost Point

John D. Bernardin
Assoc. Mem. ASME

Issam Mudawar
e-mail: mudawar@ecr.purdue.edu
Fellow ASME

Boiling and Two-Phase Flow Laboratory,
School of Mechanical Engineering,
Purdue University,
West Lafayette, IN 47907

This study presents a new mechanistic model of the Leidenfrost point (LFP); the minimum liquid/solid interface temperature required to support film boiling on a smooth surface. The model is structured around bubble nucleation, growth, and merging criteria, as well as surface cavity size characterization. It is postulated that for liquid/solid interface temperatures at and above the LFP, a sufficient number of cavities (about 20 percent) are activated and the bubble growth rates are sufficiently fast that a continuous vapor layer is established nearly instantaneously between the liquid and the solid. The model is applicable to both pools of liquid and sessile droplets. The effect of surface cavity distribution on the LFP predicted by the model is verified for boiling on aluminum, nickel and silver surfaces, as well as on a liquid gallium surface. The model exhibits good agreement with experimental sessile droplet data for water, FC-72, and acetone. While the model was developed for smooth surfaces on which the roughness asperities are of the same magnitude as the cavity radii (0.1–1.0 μm), it is capable of predicting the boundary or limiting Leidenfrost temperature for rougher surfaces with good accuracy.
[DOI: 10.1115/1.1470487]

Keywords: Boiling, Bubble Growth, Cavities, Heat Transfer

1 Introduction

The competitive demands of industry for products with enhanced material properties which can be manufactured more efficiently and with greater cost effectiveness are continually shaping and advancing processing techniques. For example, processing of aluminum alloys has received considerable attention from the automobile and aerospace industries because of such attributes as high strength-to-weight ratio, corrosion resistance, and recyclability. However, the replacement of steel components with aluminum alloy counterparts has been restricted, in part, by limited knowledge of the heat transfer aspects associated with quenching of extrusions, castings, forgings, and other heat treated parts.

Quenching involves rapid cooling of a part to control microstructural development and hence dictates material properties [1]. Figure 1 shows a typical temperature-time history of an aluminum part during a quench. The curve is divided into four distinct regimes, each possessing unique heat transfer characteristics. In the high temperature, or film boiling regime, the quench proceeds rather slowly as liquid-solid contact is prevented by the formation of an insulating vapor blanket. The lower temperature boundary of this regime is referred to as the Leidenfrost point (LFP), below which partial liquid-solid contact increases cooling rate. As discussed by Bernardin and Mudawar [1], most of the material transformations for aluminum alloys occur at temperatures above the LFP, while warping and distortions are caused by thermal stresses resulting from the large cooling rates at temperatures below the LFP. Consequently, accurate knowledge of the Leidenfrost temperature and the parameters which govern its behavior is paramount to controlling the quenching process and subsequent material properties. It must be emphasized that boiling is an interfacial phenomenon. Consequently, the Leidenfrost temperature corresponds to that of the liquid-solid interface at the LFP, which may differ significantly from temperatures within the solid.

In a previous study by the authors [2], a fairly comprehensive experimental assessment of the Leidenfrost phenomenon was performed, which included data for acetone, benzene, FC-72, and water on heated aluminum surfaces with various surface finishes. The same study also explored the effects of surface material (copper, nickel, silver, and aluminum), liquid subcooling, liquid degassing, surface roughness, and chemical residue on the Leidenfrost point. In addition, several Leidenfrost point models developed over the past four decades were reviewed and assessed. These models include hypotheses adopted from different disciplines, such as hydrodynamic instability theory, metastable physics, thermodynamics, and surface chemistry. Table 6 of Ref. [2] reveals these models fail to accurately and consistently predict the Leidenfrost temperature for sessile droplets.

The model proposed and verified in this paper is based on surface cavity size characterization as well as bubble nucleation, growth, and merging criteria. It is consistent with the relationship between surface cavities and the boiling phenomena reported in early nucleate boiling literature. In these studies, scanning electron microscopy identified micron-sized cavities on macroscopically polished surfaces and high-speed photography recorded bubble formation speculated to originate from vapor trapped within these cavities [3–5]. In conjunction with these early observations, a bubble incipience model to predict the surface superheat required to form vapor bubbles from surface cavities was developed [6–9]. The focus of continuing investigations was to correlate the observed heat flux and superheat characteristics to the number density of active cavities [4,5,10,11]. It has been well documented in these studies that as the surface superheat is increased, the number of active nucleation sites increases up to some maximum point at which bubble coalescence occurs and a vapor blanket begins to develop, covering nearly 50 percent of the surface at critical heat flux [4].

In the present study, it is hypothesized that as the Leidenfrost temperature is approached from the boiling incipience temperature, *smaller and more numerous surface cavities become activated, and the growth rate of these bubbles increases appreciably*. For liquid-solid interface temperatures at and above the LFP, a sufficient number of cavities are activated and the bubble growth rates are large enough that *liquid in immediate vicinity of the*

Contributed by the Heat Transfer Division for publication in the JOURNAL OF HEAT TRANSFER. Manuscript received by the Heat Transfer Division June 30, 2001; revision received January 7, 2002. Associate Editor: T. Y. Chu.

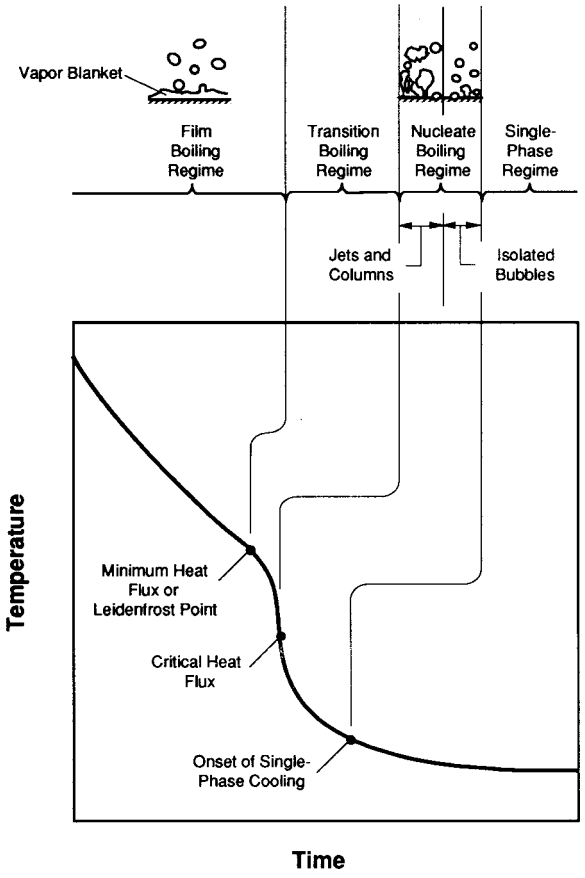

Fig. 1 Temperature-time history of a surface during quenching in a bath of liquid

surface is nearly instantaneously converted to vapor upon contact, enabling a continuous insulating vapor layer to form between the liquid and the solid.

To help explain the rationale of the proposed LFP model, Fig. 2 displays the sessile droplet evaporation time versus wall superheat, exhibiting the four distinct boiling regimes indicated in the cooling curve of Fig. 1. In this example, the interface temperature refers to that at which the liquid and the solid come in contact. Included in Fig. 2 are photographs depicting the vapor layer development for sessile water droplets approximately 2 ms after making contact with a polished aluminum surface at four interface temperatures. At an interface temperature of $T_i = 137°C$, corresponding to the transition boiling regime, individual vapor bubbles occupying roughly 15 percent of the liquid-solid contact area are visible throughout the liquid film. At 151°C, approaching the LFP, the bubble density increases significantly, covering nearly 50 percent of the droplet underside. As the interface temperature increases further, bubble density also increases, signaling the formation of a continuous vapor layer beneath the droplet. The LFP corresponds to the minimum liquid-solid interface temperature required to sustain a continuous vapor layer, as suggested in Fig. 2 for $T_i = 165°C$. At and above the LFP, the vapor layer beneath the droplet allows surface tension forces in the liquid to reduce the droplet's outer diameter noticeably as shown in Fig. 2 for $T_i = 180°C$.

To fully appreciate the proposed model, the structure of solid surfaces and its influence on the boiling process must first be explored.

Characterization of Surfaces. A typical surface is made up of many imperfections, including pits, scratches, and bumps. In addition, there is no definite region on a particular length scale which can be considered as roughness or waviness. As mentioned by Ward [12], a surface generally exhibits self-similarity, meaning that its appearance remains basically the same over a wide range of magnifications. This behavior is described in Fig. 3(*a*), in which a hypothetical surface profile is shown at various magnifications. Surface roughness features appear to repeat themselves as the magnification is increased again and again. Based on this type

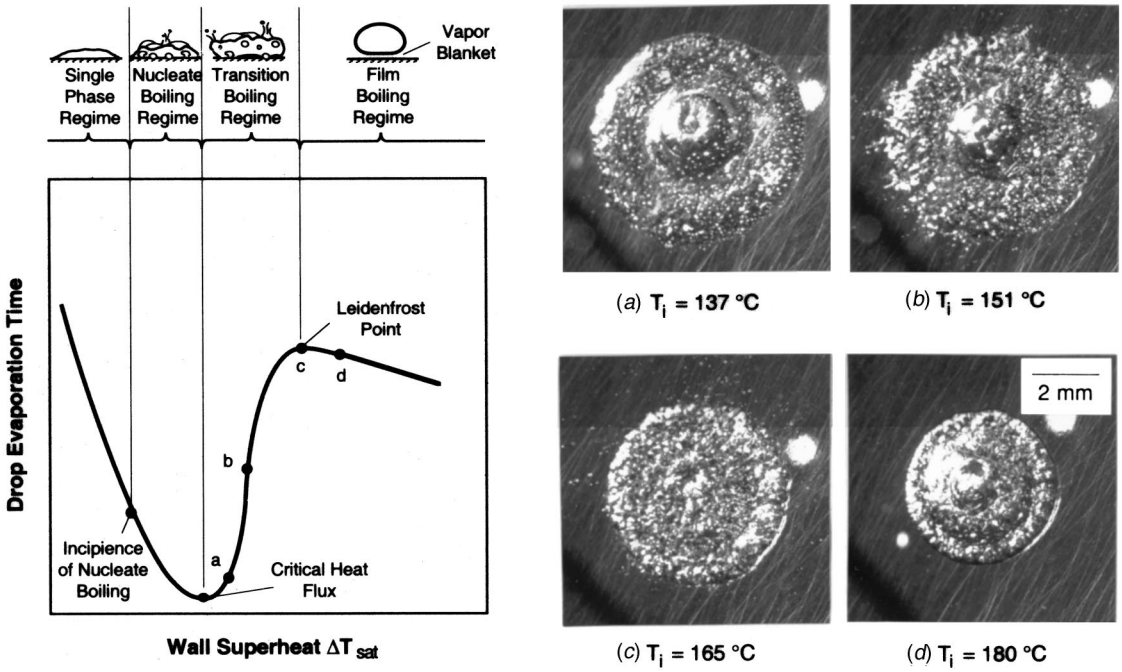

Fig. 2 Sessile droplet evaporation curve and corresponding photographs of water droplets approximately 2 ms after contact with a polished aluminum surface

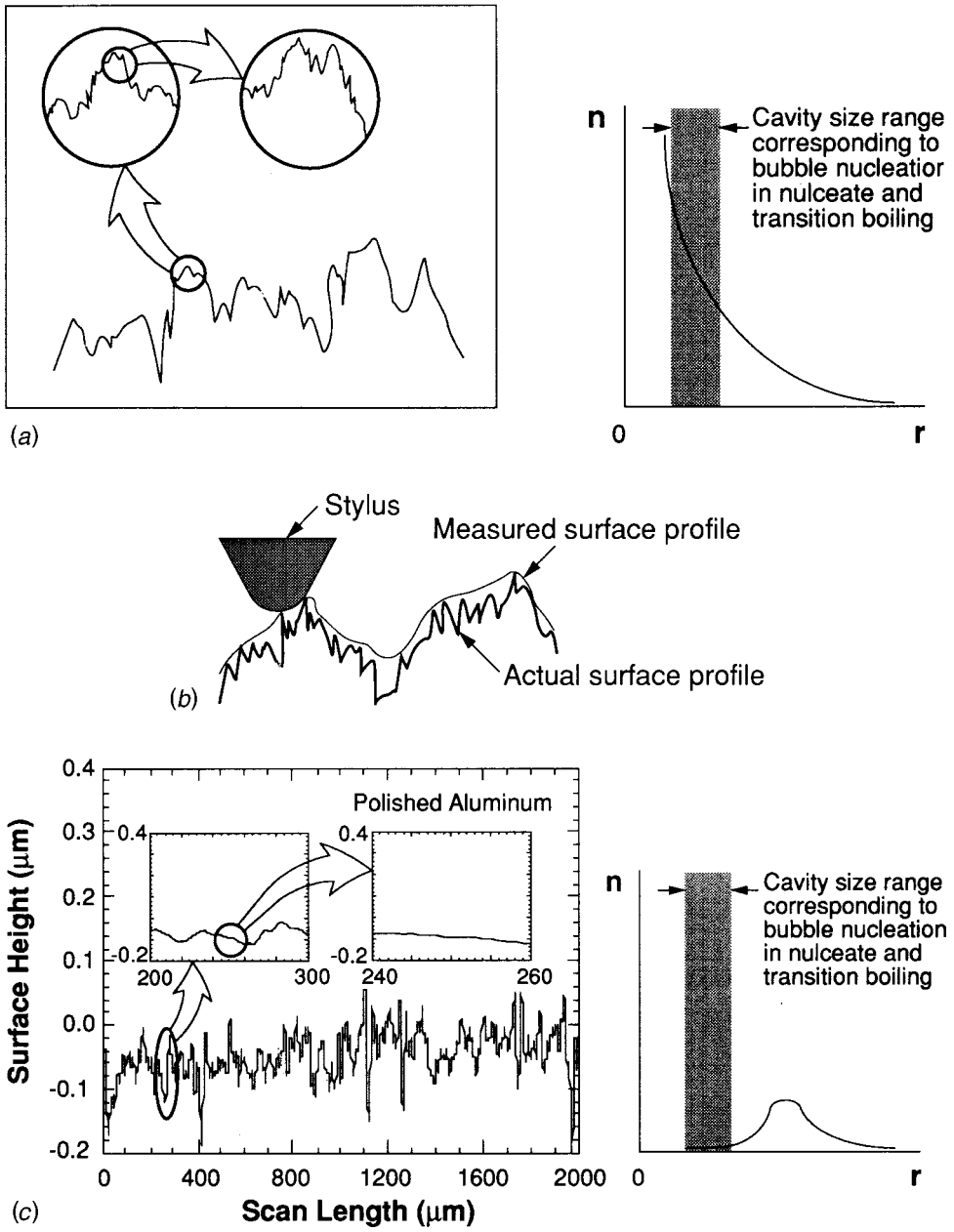

Fig. 3 Depiction of (*a*) an actual surface profile exhibiting self-similarity and the corresponding cavity size distribution, (*b*) sensitivity limitation of a stylus of a surface contact profilometer, and (*c*) a polished aluminum surface profile (with an arithmetic average surface roughness of 26 nm) measured with a contact profilometer and the corresponding cavity size distribution

of surface description, it is reasonable to conclude that the surface consists of relatively large craters, which are filled with many smaller cavities, and so on [11]. Consequently, the surface cavity sizes would be expected to fit an exponential distribution as shown in Fig. 3(*a*).

Several techniques, including surface contact profilometry, scanning electron microscopy, and various optical, electrical, and fluid methods, are available for assessing surface features [13]. As mentioned by Ward [12], each of these techniques is bandwidth limited, meaning it can only resolve surface features of a certain size interval. Figures 3(*b*) and 3(*c*) describe this limitation for a surface contact profilometer, showing how at higher magnifications the surface appears to get smoother as fine surface features are no longer detected. This resolution limit is the result of the physical size of the diamond stylus, typically having a tip radius of 1 to 10 μm. Thus, the resulting surface cavity distribution measured with such an instrument would erroneously exhibit the characteristic dome-shape of Fig. 3(*c*) commonly employed in boiling heat transfer literature. Cavities which serve as bubble nucleation sites (0.1 to 5 μm) would not be detected with a surface contact profilometer [2,11].

Scanning electron microscopy images (SEMS) help identify and characterize the cavities which serve as nucleation sites. Figure 4 displays surface cavity distributions for a polished aluminum surface determined from SEMS at two different magnifications. Each distribution is limited by the SEM magnification. However, by combining the distributions from both SEMS, a complete cavity size distribution covering the range responsible for bubble nucleation of common fluids is obtained.

In the past, a number of investigations were performed to char-

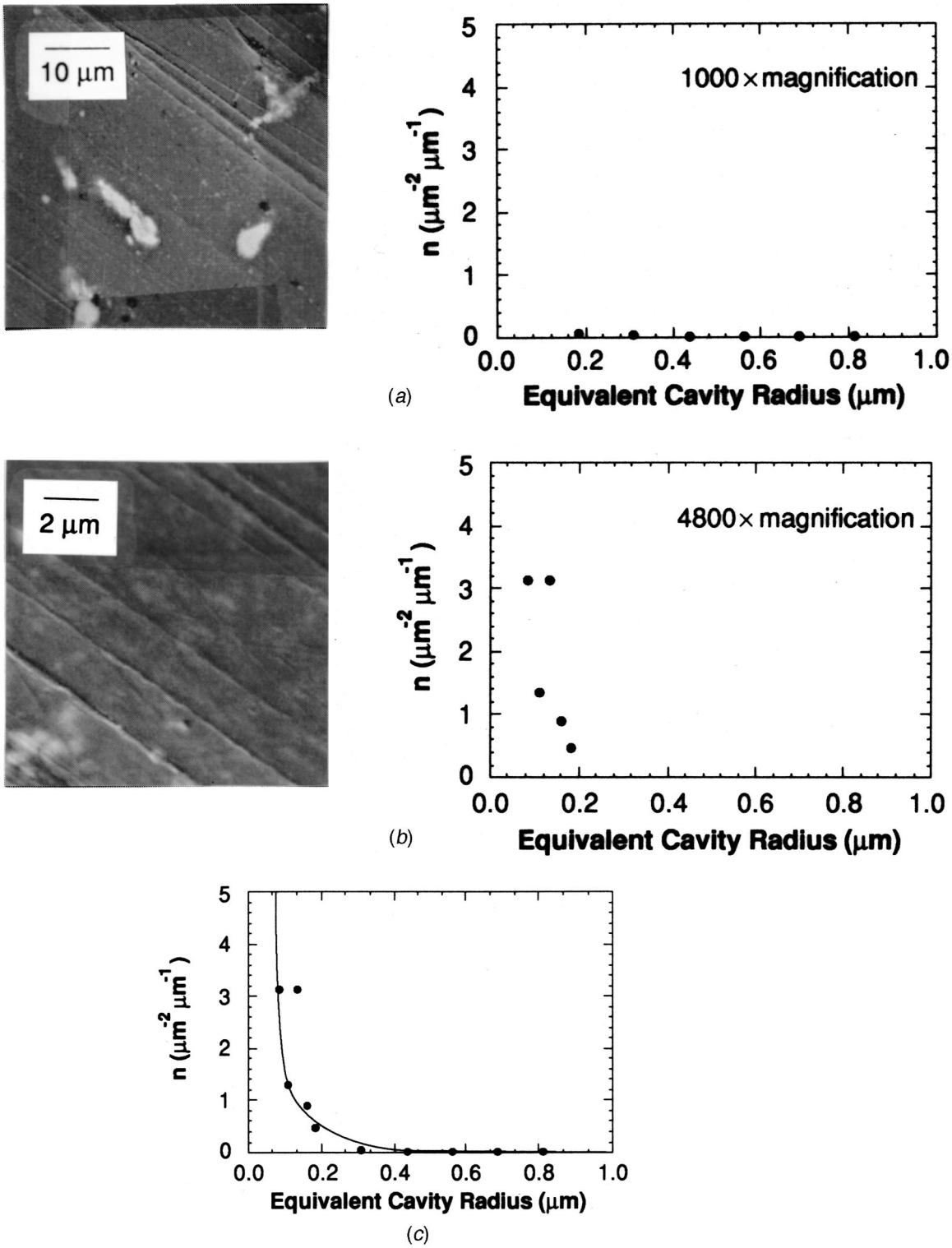

Fig. 4 Cavity size distributions for a polished aluminum surface determined from scanning electron microscopy images at (*a*) 1000× magnification, (*b*) 4800× magnification, and (*c*) combined magnifications

acterize surface features responsible for nucleate boiling to derive quantitative relationships for nc_a, the number of surface cavities which are activated [11,14–16]. More recently, Yang and Kim [17] determined nc_a using scanning electron and differential interference microscope data along with the vapor entrapment criterion (contact angle, θ, must be greater that the cone angle, ϕ, of the assumed conical-shaped cavities). Later, Wang and Dhir [18] determined the relationship between the number of surface cavities per unit area, nc, and those that become activated, nc_a, for water boiling on a polished copper surface. They also confirmed Gaertner's [19] statistical spatial distribution of active cavities. Using a Poisson distribution function, Gaertner derived the fol-

lowing expressions for the statistical distribution, $f(d)$, and average, $\bar{d}$, of nearest-neighbor distances, d, between cavities

$$f(d) = 2\pi n c_a d \exp(n c_a \pi d^2) \tag{1}$$

$$\bar{d} = \frac{0.50}{\sqrt{n c_a}}. \tag{2}$$

The remainder of this paper presents the development of the new theoretically-based LFP model. Experimental data and numerical schemes required to solve the model equations are included and discussed. Finally, comparisons are made between the model predictions and empirical data to demonstrate both the robustness and accuracy of this model.

2 LFP Model Development

The methodology used to construct the present LFP model relies upon two important aspects concerning bubble nucleation and its relationship to surface temperature and cavity shape and distribution. First, based upon earlier bubble nucleation criteria [6–9], increasing surface superheat beyond the boiling incipience temperature causes both larger and smaller surface cavities to activate and bubble growth rates to increase. Secondly, for a typical polished surface, there is an exponential increase in the number of surface cavities with decreasing cavity mouth radius [17,18], as shown in Fig. 3.

In the present study, the authors postulate that at some large liquid-solid interface temperature corresponding to the LFP, a sufficient number of cavities will activate to produce enough vapor to separate the liquid from the solid, and hence, induce film boiling. Discussed below are the various sub-models used to support the overall LFP model. In the next section, a solution procedure based upon these sub-models is outlined.

Bubble Nucleation. The criteria for bubble nucleation from cavities have been rigorously investigated theoretically and verified experimentally by many researchers. The significant aspects of the bubble nucleation model are outlined below. In the development that follows, it is assumed that the surface cavities are conical.

The pressure drop across a spherical bubble interface of radius r is given as

$$P_g - P_f = \frac{2\sigma}{r}. \tag{3}$$

A relation for the liquid superheat, ΔT_{sat}, required to provide the necessary gas pressure, P_g, for initiation of bubble growth can be found by integrating the Clausius-Clapeyron equation along the saturation line,

$$\int_{P_{f,\text{sat}}}^{P_{g,\text{sat}}} dP = \int_{\tau_{\text{sat}}}^{T_{\text{sat}}+\Delta T_{\text{sat}}} \frac{h_{fg}}{T v_{fg}} dT. \tag{4}$$

By substituting Eq. (3) for the pressure difference ($P_{g,\text{sat}} - P_{f,\text{sat}}$) and holding the latent heat of vaporization and specific volume difference constant, Eq. (4) can be integrated to give the following expression for the surface superheat temperature required to initiate the growth of a hemispherical vapor bubble of radius r,

$$T_{\text{rsh}} = T_{\text{sat}} \exp\left(\frac{2\sigma v_{fg}}{r h_{fg}}\right). \tag{5}$$

By assuming constant values for h_{fg} and v_{fg} (evaluated at the mean temperature $(T_{\text{rsh}} + T_{\text{sat}})/2$), integrating Eq. (4) produces a difference of only 6 percent (for water and a surface superheat temperature of 190 °C) from the results obtained by substituting temperature-dependent properties and performing the more complicated integration.

The superheat available for bubble nucleation is provided by the transient heat diffusion following contact of the liquid with the heated surface. For a relatively short duration over which rapid bubble nucleation occurs at high superheats, the contact between the liquid and solid can be modeled as one-dimensional transient conduction between two semi-infinite bodies. The transient temperature distribution in the liquid, or the available superheat, $T_{\text{ash}}(y,t)$, is given by [20]

$$T_{\text{ash}} = T_i + (T_f - T_i)\text{erf}\left(\frac{y}{2\sqrt{\alpha_f t}}\right). \tag{6}$$

where the interface temperature, T_i, is

$$T_i = \frac{(k\rho c_p)_s^{1/2} T_s + (k\rho c_p)_f^{1/2} T_f}{(k\rho c_p)_s^{1/2} + (k\rho c_p)_f^{1/2}}. \tag{7}$$

y is the distance into the liquid measured normal to the liquid-solid interface, and T_s and T_f are, respectively, the surface and liquid temperatures prior to the contact.

The minimum condition necessary for bubble nucleation is met when the available superheat at a distance y from the solid surface, is equal to the required superheat for a hemispherical bubble whose radius, r, is equal to y. This condition is represented by equating the required and available superheats from Eqs. (5) and (6), respectively:

$$T_{\text{sat}} \exp\left(\frac{2\sigma v_{fg}}{r h_{fg}}\right) = T_i + (T_f - T_i)\text{erf}\left(\frac{r}{2\sqrt{\alpha_f t}}\right). \tag{8}$$

Cavity Size Distribution. Surface cavities and other defects, typically on the order of 1 to 10 μm, have long been known to be highly influential in controlling nucleate boiling by serving as nucleation sites. In this study, scanning electron microscopy (SEM) was utilized to characterize the surface cavity distributions of macroscopically polished surfaces from which empirical Leidenfrost temperature measurements were made [2]. NIH Image, an image processing and analysis program for the Macintosh was utilized in conjunction with digitized SEM images of the polished surfaces to determine the number and sizes of the surface cavities. The program determined the mouth area of each irregular cavity, and then calculated an equivalent circular cavity mouth radius which would provide an equal mouth area.

From inspection of various SEM images at different magnifications, it was apparent that the number of cavities per unit area, n, having an equivalent mouth radius between r and $r + \Delta r$, could be fit by the exponential function

$$n = a_1 \exp(-a_2 r). \tag{9}$$

Using the scanning electron microscopy images of the various surfaces used in this study, the following curve fits were obtained over a cavity size range of 0.07 to 1.0 μm:

$$n = 3.379 \exp(-10.12r) \quad \text{(aluminum)} \tag{10a}$$

$$n = 4.597 \exp(-12.20r) \quad \text{(nickel)} \tag{10b}$$

$$n = 13.16 \exp(-16.07r) \quad \text{(silver)}, \tag{10c}$$

where the units for n and r are sites.μm^{-2}.μm^{-1} and μm, respectively. The curve fits had acceptable least square residuals with a worst case value of 0.87.

The cumulative number of surface cavities in the radius interval $r_{\min} \leqslant r \leqslant r_{\max}$, is then obtained through integration,

$$nc = \int_{r_{\min}}^{r_{\max}} n(r)dr = \frac{a_1}{a_2}[\exp(-a_2 r_{\min}) - \exp(-a_2 r_{\max})]. \tag{11}$$

Bubble Growth. Due to the relatively high superheat and short duration over which vapor is created in the film boiling regime, it is believed the rapid bubble growth will be initially dominated by inertia rather than heat diffusion. For this condition, bubble growth is described by the Rayleigh equation (neglecting

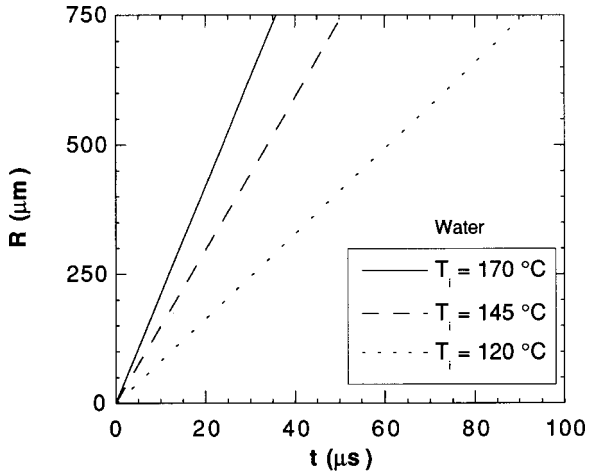

Fig. 5 Temperature dependence of vapor bubble growth for water as predicted by the numerical solution to the Rayleigh equation

viscous effects) which can be derived from the momentum equation for incompressible and irrotational flow [21], or from energy conservation principles [22], incorporating the pressure drop across a spherical interface, $2\sigma/R$.

$$R\ddot{R}+\frac{3}{2}\dot{R}^2=\frac{1}{\rho_f}\left[(P_g-P_\infty)-\frac{2\sigma}{R}\right], \tag{12}$$

where $\dot{R}$ and $\ddot{R}$ are, respectively, the first and second derivatives of bubble radius with respect to time, and P_∞ is the liquid pressure far from the bubble interface. While no analytical solution to the Rayleigh equation exists, an asymptotic solution ($R \gg R_o$) which neglects surface tension forces, has been obtained [22,23].

However, for early stages of bubble growth, surface tension forces cannot be neglected. Consequently, Eq. (12) must be solved to accurately describe these early stages of bubble growth. In solving the differential Rayleigh equation, the following intermediate step

$$d(R^{3/2}\dot{R})=\frac{1}{\rho_f}\left(\Delta P-\frac{2\sigma}{R}\right)R^{1/2}dt=\frac{1}{R^{3/2}\dot{R}}d\left[\frac{\Delta P}{\rho_f}\frac{R^3}{3}-\frac{\sigma R^2}{\rho_f}\right] \tag{13}$$

was used in the present study to reduce Eq. (12) to the following integral

$$t=\int_0^R\frac{dR}{\left[\frac{2}{3\rho_f}(P_g-P_\infty)-\frac{2\sigma}{\rho_f R}\right]^{0.5}} \tag{14}$$

Figure 5 displays the numerically predicted temperature dependence for bubble growth for surface temperatures corresponding to nucleate, transition, and film boiling of water. As expected, the growth rate increases appreciably with increasing surface temperature.

The bubble growth predicted by Eq. (14) is similar to the rapid inertia-controlled growth examined numerically and analytically by Lee and Merte [24] and Bankoff and Mikesell [26], respectively. The bubble growth rates displayed in Fig. 5 are also very similar to data for bubble growth in superheated water presented in the same references. The hemispherical bubble geometry adopted in the present model for the inertia-controlled growth is consistent with the description given by Carey [27].

Interaction of the Thermal Boundary Layer and the Growing Bubbles. As will be shown in the next section, the bubble growth predicted by the numerical solution to the Rayleigh equation is several orders of magnitude faster than that of the thermal boundary layer. Therefore, it is assumed the early stage of bubble growth is described by the solution to the Rayleigh Eq. (14) until the bubble dome reaches the maximum bubble stability point in the growing thermal boundary layer predicted by Eq. (8), after which the bubble growth is controlled by this slower diffusion rate of the thermal boundary layer. This two-staged bubble growth model is fairly consistent with the numerical bubble growth model of Lee and Merte [24], which predicts a rapid inertia-controlled bubble growth that converges to a much slower thermally controlled growth as the bubble expands.

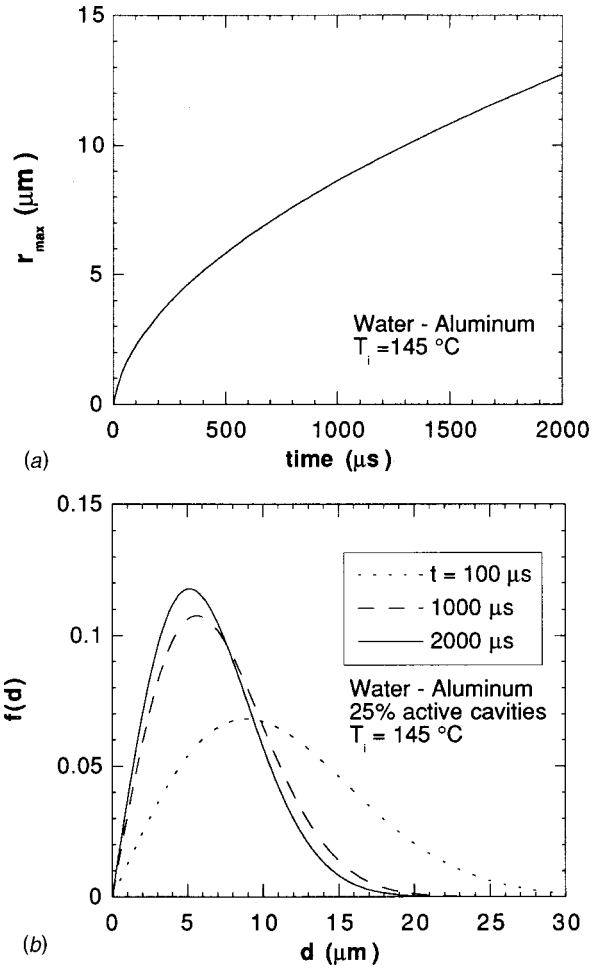

Fig. 6 (*a*) Transient maximum cavity activation and bubble radius and (*b*) nearest-neighbor cavity distances for 25 percent cavity activation at three different times following liquid-solid contact for water on a polished aluminum surface with an interface temperature of 145°C

At interface temperatures well above the boiling point of the liquid, the number of active surface cavities and the bubble growth rates can become significantly large that bubble interference begins to take place. Figure 6 describes this interference for water in contact with a polished aluminum surface with an interface temperature of 145°C. Figure 6(*a*) displays the transient maximum stable bubble radius supported by the growing thermal boundary layer as predicted by Eq. (8). Figure 6(*b*) shows the nearest-neighbor distance distribution given by Eq. (1) and the transient cumulative cavity density for a polished aluminum surface 100, 1000, and 2000 μs following liquid-solid contact. In Fig. 6(*b*), it is assumed that only 25 percent of the surface cavities satisfy the vapor entrapment criterion and serve as nucleation sites, an estimate consistent with the findings of Yang and Kim [17] and Wang and Dhir [18].

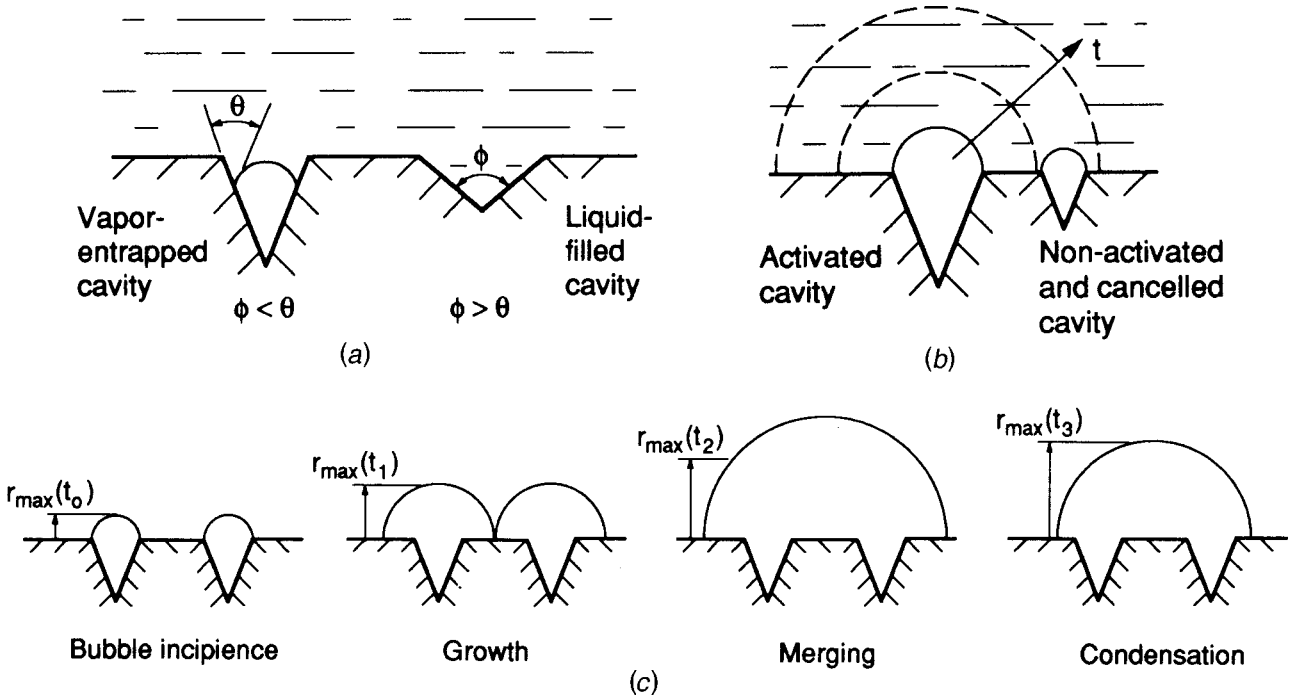

Fig. 7 Schematic representation of different forms of cavity cancellation: (*a*) poor vapor entrapment, (*b*) neighbor bubble overgrowth, and (*c*) bubble merging

In comparing Figs. 6(*a*) and 6(*b*), it is apparent that the bubble radius exceeds half of the nearest-neighbor distance for a large percentage of the active cavities, a condition which is necessary for two bubbles to interfere with one another. This trend increases significantly as time progresses. However, not all cavities will participate equally in this process. Because of several cancellation effects discussed below, only a small fraction of the cavities will activate to form bubbles which grow until they begin to interfere with bubbles from neighboring cavities.

Figure 7 is a schematic representation of different forms of surface cavity cancellation which occur before or during the development of the vapor layer. Figure 7(*a*) displays the vapor entrapment mechanism for conical surface cavities. When the liquid initially makes contact with the solid surface, only those cavities with a cone angle smaller than the advancing contact angle will entrap vapor and serve as bubble nucleation sites [25]. Two other types of cavity cancellation occur during bubble growth from nucleation sites. As illustrated in Fig. 7(*b*), a bubble from an activated cavity can overgrow a non-activated, vapor entrapped cavity, thus canceling it out as a nucleation site. Two growing bubbles may collide and merge as depicted in Fig. 7(*c*). In this case, the bubbles, represented as hemispheres for simplicity, may form a single larger bubble which extends beyond the stability limit of the thermal boundary layer, causing condensation and bubble shrinkage to temporarily occur. The net effect is the cancellation of an active bubble source by bubble merging.

It should be noted that the LFP model described in this paper is applicable to sessile as well as impinging droplets. In addition, since the model is constructed around cavity activation and bubble growth arguments, and not on the expanse of the surrounding liquid, it should be applicable to pool boiling as well.

3 LFP Model Solution Procedure

Upon contact between a sessile droplet and a heated surface, a thermal boundary layer begins to develop in the liquid. At some time t_o, the thermal boundary layer would have grown sufficiently large to satisfy the bubble nucleation criterion for conical-shaped cavities with a mouth radius r_o as shown in Fig. 8(*a*). For a polished surface, this radius is typically well within the range of cavity radii available on the surface. As time progresses and thermal boundary layer thickens, all cavities within a specific cavity radius interval are activated. This interval is given by the two roots of Eq. (8), namely, $r_{\min}(t)$ and $r_{\max}(t)$, as displayed in Fig. 8(*b*), where $r_{\max}$ is the radius of the largest activated cavity at a given instant, not the largest cavity on the surface. Similarly, $r_{\min}$ is the smallest activated cavity.

Table 1 presents curve fits for $r_{\min}(t)$ and $r_{\max}(t)$ obtained by solving Eq. (8) over a 2 ms time interval for a variety of fluids and liquid-solid interface temperatures. These curve fits were used in the remainder of the LFP model calculations to determine the Leidenfrost temperature for sessile droplets.

Assuming only a fraction, ψ, of the cavities actively participate in the growth of the vapor layer due to the cancellation effects described in the previous section, and that bubbles grow from cavities as hemispheres, the time dependence of the cumulative number of activated cavities per unit area can be found by integrating the cavity size distribution over the radius limits $r_{\min}(t)$ and $r_{\max}(t)$:

$$nc_a(t) = \psi \int_{r_{\min}(t)}^{r_{\max}(t)} a_1 \exp(-a_2 r)\, dr$$

$$= \psi \frac{a_1}{a_2} \{\exp(-a_2 r_{\min}(t)) - \exp(-a_2 r_{\max}(t))\}. \quad (15)$$

Since the inertia-controlled bubble growth rate predicted by Eq. (14) is orders of magnitude greater than the thermal boundary layer growth rate, it is assumed all bubbles initiated with $r_o < r_{\max}(t)$ will rapidly grow to $r_{\max}(t)$, the maximum stable hemispherical bubble radius supported by the growing thermal boundary layer. A hemispherical bubble will not be stable for sizes beyond $r_{\max}(t)$ as condensation on the leading front of the growing bubble would significantly reduce its growth rate [26]. This is consistent with bubble incipience model of Hsu [7] and the experimental results of Clark et al. [3]. Consequently, the limiting condition considered here is that once the bubbles reach the thermal boundary layer limit of $r_{\max}(t)$ they will continue to grow at

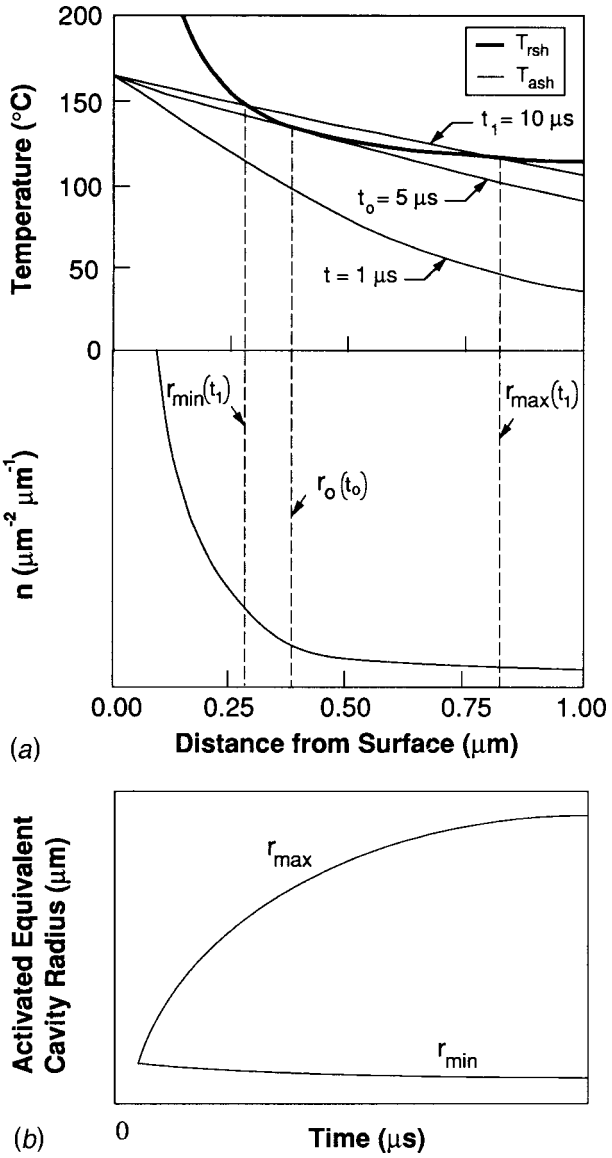

Fig. 8 Transient cavity nucleation model including (*a*) cavity nucleation superheat criteria and corresponding cavity size distribution with transient activation window, and (*b*) transient maximum and minimum active cavity radii for water in contact with a hot surface with an interface temperature of 165°C

the same rate as the thermal boundary layer, i.e., $\dot{r}_{max}(t)$. This two-stage growth is consistent with the bubble growth findings of Lee and Merte [24].

Given this bubble growth model, the time-dependent percent area coverage of the liquid-solid interface by vapor, $AB\%(t)$, is then given by

$$AB\%(t) = nc_a(t)\pi r_{max}^2(t) \tag{16}$$

which, upon substitution of Eq. (15), gives

$$AB\%(t) = \psi \frac{a_1}{a_2}\{\exp(-a_2 r_{min}(t)) - \exp(-a_2 r_{max}(t))\}\pi r_{max}^2(t). \tag{17}$$

To determine the cavity cancellation parameter, ψ, in Eq. (17), the vapor layer development in Fig. 2 corresponding to 137°C was compared to vapor layer predictions of the LFP model. A value of 0.05 for ψ resulted in a 15 percent vapor layer coverage, consistent with the 14.5 percent value for $T_i = 137$°C in Fig. 2 determined with the image analysis software. A value of 0.05 for ψ indicates that even if 25 percent of the cavities satisfy the vapor entrapment criterion, as discussed previously and illustrated in Fig. 6, only 20 percent of these nucleation sites actively participate in the vapor layer growth; the remaining sites being canceled out by the effects illustrated in Fig. 7. Based on this comparison, a value of 0.05 for ψ was used consistently for all subsequent calculations presented in this study. Due to the complex shapes of surface features and the limited means of analyzing these shapes, it is extremely difficult to characterize the surface cavities which serve as potential nucleation sites. In addition, the contact angle used for the vapor entrapment criterion is highly dependent on the spreading velocity of the liquid, surface contamination, as well as surface roughness [28]. Since the present models for surface characterization and bubble nucleation are limited in their degree of accuracy, a more accurate means of determining the percent of actively participating surface cavities, ψ, is currently unavailable and warrants further investigation. Nevertheless, it should be emphasized that while the choice of ψ will influence the vapor layer growth rate, the strong temperature-dependence of the latter, $\Delta AB\%/\Delta t$, which is used to identify the LFP in the present model, is still very well preserved.

Table 1 Active cavity radii equations for sessile droplets of various liquids in contact with a hot surface for different interface temperatures

Fluid (T_{sat} °C)	T_i (°C)	r_{min} (μm)	r_{max} (μm)
Acetone (56)	95	$0.200\ t^{-0.022}$	$0.275\ t^{0.511}$
	115	$0.097\ t^{-0.015}$	$0.349\ t^{0.506}$
	135	0.051	$0.401\ t^{0.505}$
FC-72 (56)	70	$1.085\ t^{-0.161}$	$0.037\ t^{0.661}$
	85	$0.168\ t^{-0.032}$	$0.148\ t^{0.532}$
	100	$0.081\ t^{-0.012}$	$0.207\ t^{0.512}$
	115	$0.049\ t^{-0.010}$	$0.242\ t^{0.506}$
Water (100)	145	$0.606\ t^{-0.051}$	$0.162\ t^{0.573}$
	165	$0.251\ t^{-0.019}$	$0.304\ t^{0.521}$
	185	$0.141\ t^{-0.012}$	$0.389\ t^{0.509}$

4 LFP Model Assessment

Figure 9(*a*) shows the temperature dependence of the transient vapor layer growth for a sessile water droplet on a polished aluminum surface with the cavity distribution given by Eq. (10*a*). The time for complete vapor layer development ($AB\% = 100$) is shown to rapidly decrease as the interface temperature is increased from 145 to 185°C. While the model predicts an eventual 100 percent vapor layer growth for the interface temperature of 145°C, other effects such as bubble departure and liquid motion which are not accounted for in the model, would interrupt this development within a few milliseconds of liquid-solid contact,

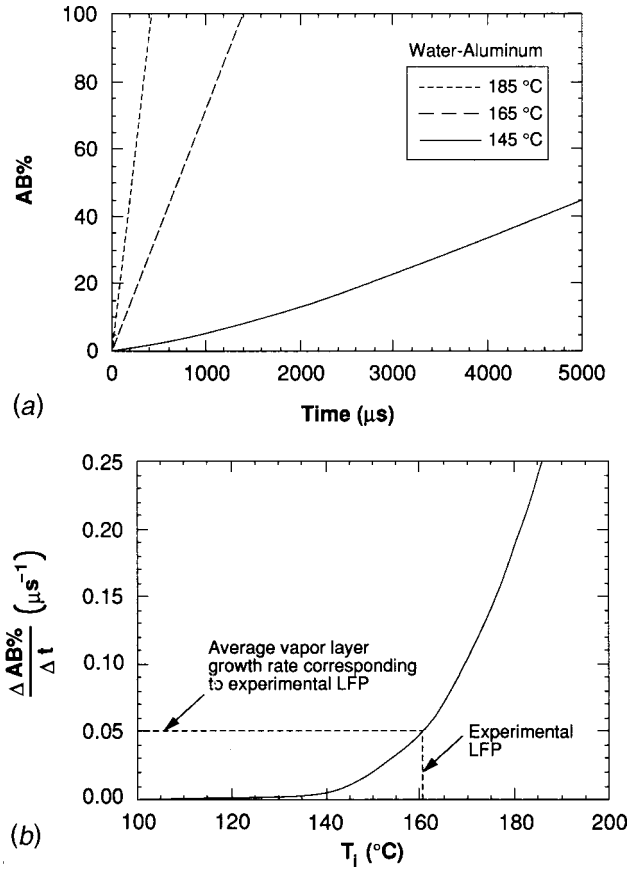

Fig. 9 Temperature dependence of the (*a*) transient vapor layer coverage and (*b*) average vapor layer growth rate for a sessile water droplet on a polished aluminum surface

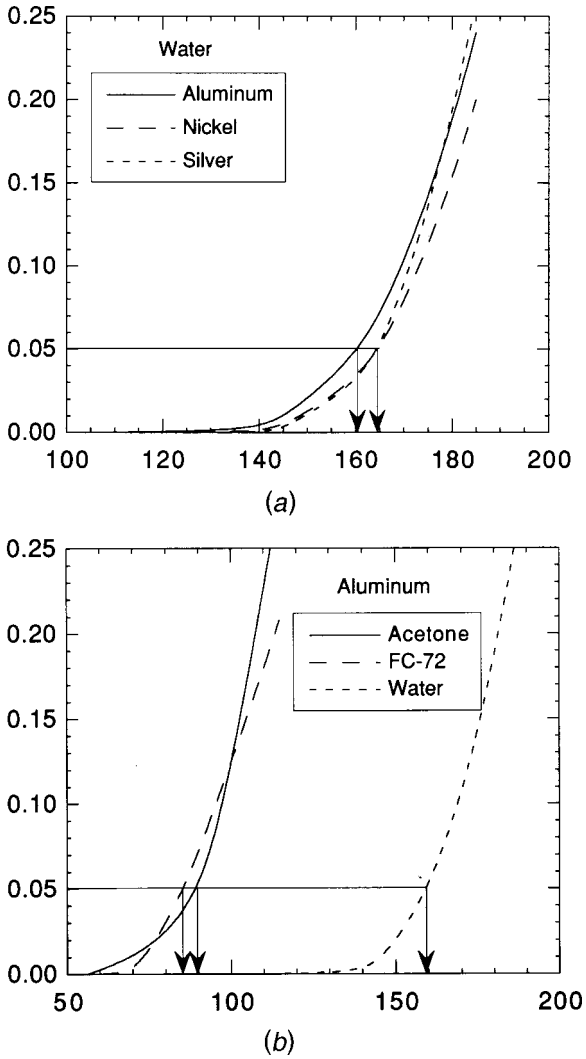

Fig. 10 Average vapor layer growth rate for sessile droplets of (*a*) water on various polished metallic surfaces and (*b*) acetone, FC-72, and water on polished aluminum

and hence prevent film boiling from occurring. Figure 9(*b*) presents the trend observed in Fig. 9(*a*) in a slightly different manner. Figure 9(*b*) shows that as the interface temperature increases beyond the liquid saturation temperature, the average vapor layer growth rate will increase exponentially. Intuition suggests that at some minimum interface temperature, the LFP, the average vapor layer growth rate will become sufficiently high to support film boiling. To determine the minimum average vapor layer growth rate required to support film boiling, experimental LFP data for sessile water droplets on aluminum were employed. The water-aluminum system was used earlier in the model development to determine the percentage of actively participating surface cavities and this system was also highly scrutinized in an experimental study of the LFP [2]. Shown in Fig. 9(*b*) is the experimentally determined Leidenfrost temperature of 162°C ($T_s = 170$°C) for sessile water droplets on aluminum which corresponds to an average vapor layer growth rate of 0.05. This value of the average vapor layer growth rate was used throughout the LFP model assessment of different liquid-solid systems.

This same technique, as described by Carey [27], has been used to determine the critical vapor bubble formation rate needed to sustain homogeneous nucleation within a superheated liquid. In the homogeneous nucleation superheat limit model, the vapor bubble formation rate increases exponentially with increasing liquid temperature, much like the vapor blanket growth rate in the present study. Carey explains how empirical data were used to determine a critical vapor bubble formation rate, and how this single bubble formation rate was used to determine the homogeneous nucleation superheat limit of several different liquids including water.

Figures 10(*a*) and 10(*b*) display, respectively, the average vapor layer growth rate versus interface temperature for sessile water droplets on various metallic surfaces and sessile acetone, FC-72, and water droplets on aluminum. Using these plots and an average vapor layer growth rate of 0.05, the LFP was determined for each of these fluid-solid systems. These LFP model predictions are compared to measured values [2] in Table 2. Excellent agreement is obtained for all cases except acetone, where the agreement is only fair. Even so, these results are quite promising considering the large differences in the wetting characteristics as well as the thermodynamic and thermal properties of the fluids and solids used in the comparison. In addition, the differences between the LFP predictions and present measurements are significantly smaller than the majority of previous LFP predictive tools presented in [2]. The difference exhibited for acetone on aluminum may be due to the limitation imposed on the number of actively participating cavities, accounted for in the parameter ψ in Eq. (17). As discussed earlier, the existing techniques for modeling vapor entrapment and bubble nucleation as well as characterization of surface cavities are limited and warrant continued study. Adopting newer techniques may lead to a more accurate means of determining the number of actively participating cavities and hence further strengthen the present LFP model.

Table 2 Comparison of measured Leidenfrost temperatures [2] and predictions based on the present LFP model for acetone, FC-72, and water on various polished metallic surfaces

Fluid	Polished Surface Material	T_{leid} (°C) (LFP model)	T_{leid} (°C) (measured)
Acetone	Aluminum	90	132
FC-72	Aluminum	87	89
Water	Nickel	165	161
	Silver	165	169
	Aluminum	162	162

Further Justifications of the LFP Model and Application to Rough Surfaces. For a perfectly smooth surface which is void of all surface cavities, the current LFP model predicts that the liquid can be heated to an infinitely high temperature and film boiling would never be reached. Realistically, the maximum temperature that the liquid can be heated to, above which it is instantaneously converted to vapor, is referred to as the kinetic or thermodynamic superheat limit. Methods to predict this superheat limit, which is well above the Leidenfrost temperature of the liquid-solid systems presented earlier in this study, can be found elsewhere [29].

Gallium, a liquid metal with a melting point of 29.8°C and density of 5900 kg.m^{-3}, was used in the present study to provide a smooth liquid surface nearly free of defects. Using a thermal monitoring system consisting of a temperature controller, cartridge heater, and thermocouple, sessile droplet evaporation experiments, similar to those described in [2], were performed to determine the LFP of water on liquid gallium. Results revealed a gallium temperature of 260°C was needed to provide a water/gallium interface temperature of 222°C corresponding to the LFP. Impurities in the gallium caused by oxidation and contaminant metals were speculated to provide a few heterogeneous nucleation sites which prevented the water from obtaining its maximum superheat temperature limit of 273°C predicted using the thermodynamic homogeneous nucleation model [30], or 310°C according to the kinetic homogeneous nucleation model [27]. However, the results do indicate that a dramatic reduction in surface cavities greatly increases the Leidenfrost temperature, which is in agreement with the present LFP model.

While this model was developed for polished surfaces, it also provides a limiting condition for surfaces possessing roughness features orders of magnitude larger than the cavity radii responsible for bubble nucleation (0.1 to 1 μm). The model effectively predicts a lower limit to the Leidenfrost temperature for sessile droplets and pools of liquid. Contamination and surface roughness will act to increase the Leidenfrost temperature by requiring a thicker vapor layer to inhibit liquid-solid contact. This is supported by experimental data for sessile droplets of different liquids on surfaces of various roughnesses [2].

5 Conclusions

This study presented a new theoretically based LFP model which was constructed around vapor bubble nucleation, growth, and interference criteria, along with surface cavity size characterization. After evaluating the model with an extensive experimental database, the following key conclusions can be drawn about its validity and use:

1. The number of surface cavities which act as bubble nucleation sites increases exponentially with increasing liquid-solid interface temperature.
2. Bubble growth rates predicted by the solution to the Raleigh equation are several orders of magnitude greater than the growth rate of the thermal boundary layer for conditions consistent with film boiling of common fluids. Consequently, the bubbles emanating from active surface cavities grow instantaneously to the maximum allowable radius as predicted by bubble nucleation theory, and thereafter, grow at the rate of the diffusing thermal boundary layer.
3. For interface temperatures at and above the LFP, the present model predicts the number of active sites and bubble growth rates are large enough that a complete vapor layer is established between the liquid and solid almost instantaneously upon contact.
4. The present model is substantiated by a large experimental data base for sessile droplets, provided the surface roughness features are on the same order of magnitude as the cavities responsible for bubble nucleation. For rougher surfaces, the model predicts a lower bound for the sessile droplets.

Acknowledgment

The authors gratefully acknowledge the support of the Office of Basic Energy Sciences of the U.S. Department of Energy (Grant No. DE-FE02-93ER14394.A003).

Nomenclature

a_1, a_2 = coefficients in cavity size distribution
AB % = percent liquid-solid interface area coverage by vapor
c_p = specific heat at constant pressure
$\underline{d}$ = nearest-neighbor cavity distance
$\overline{d}$ = average nearest-neighbor cavity distance
$f(d)$ = nearest-neighbor cavity distance distribution
h_{fg} = latent heat of vaporization
k = thermal conductivity
n = number of surface cavities per unit area per unit interval (sites μm^{-2} μm^{-1})
nc = cumulative number of surface cavities per unit area (sites μm^{-2})
nc_a = cumulative number of active surface cavities per unit area (sites μm^{-2})
P = pressure
R = bubble radius
$\dot{R}$ = first derivative of bubble radius with respect to time
$\ddot{R}$ = second derivative of bubble radius with respect to time
r = surface cavity radius
r_a = radius of active surface cavity (μm)
T = temperature
t = time
v_{fg} = specific volume difference between vapor and liquid
y = normal distance from solid surface

Greek Symbols

α = thermal diffusivity
ΔAB %/Δt = average vapor layer growth rate
ΔT_{sat} = surface superheat, $T_s - T_{sat}$
ϕ = cavity cone angle
θ = contact angle
ρ = density

σ = surface tension
ψ = fraction of actively participating cavities

Subscripts

a = active
ash = available superheat
f = liquid
g = vapor
i = liquid-solid interface
leid = Leidenfrost condition
max = maximum
min = minimum
o = initial, nucleation
rsh = required superheat
s = surface, solid
sat = saturation
∞ = liquid condition far from bubble interface.

References

[1] Bernardin, J. D., and Mudawar, I., 1995, ''Validation of the Quench Factor Technique in Predicting Hardness in Heat Treatable Aluminum Alloys,'' Int. J. Heat Mass Transf., **38**, pp. 863–873.
[2] Bernardin, J. D., and Mudawar, I., 1999, ''The Leidenfrost Point: Experimental Study and Assessment of Existing Models,'' ASME J. Heat Transfer, **121**, pp. 894–903.
[3] Clark, H. B., Strenge, P. S., and Westwater, J. W., 1959, ''Active Sites for Nucleate Boiling,'' Chem. Eng. Prog., Symp. Ser., **55**, pp. 103–110.
[4] Gaertner, R. F., and Westwater, J. W., 1959, ''Population of Active Sites in Nucleate Boiling Heat Transfer,'' Chem. Eng. Prog., Symp. Ser., **55**, pp. 39–48.
[5] Kurihara, H. M., and Myers, J. E., 1960, ''The Effects of Superheat and Surface Roughness on Boiling Coefficients,'' AIChE J., **6**, pp. 83–91.
[6] Bankoff, G. S., 1959, ''The Prediction of Surface Temperatures at Incipient Boiling,'' Chem. Eng. Prog., Symp. Ser., **55**, pp. 87–94.
[7] Hsu, Y. Y., 1962, ''On the Size Range of Active Nucleation Cavities on a Heating Surface,'' ASME J. Heat Transfer, **84**, pp. 207–213.
[8] Han, C. Y., and Griffith, P., 1965, ''The Mechanism of Heat Transfer in Nucleate Pool Boiling-Part I,'' Int. J. Heat Mass Transf., **8**, pp. 887–904.
[9] Lorenz, J. J., Mikic, B. B., and Rohsenow, W. M., 1974, ''The Effects of Surface Condition on Boiling,'' *Proc. Fifth Int. Heat Transfer Conf.*, **4**, Tokyo, pp. 35–39.
[10] Gaertner, R. F., 1965, ''Photographic Study of Nucleate Pool Boiling on a Horizontal Surface,'' ASME J. Heat Transfer, **87**, pp. 17–29.
[11] Cornwell, K., and Brown, R. D., 1978, ''Boiling Surface Topography,'' *Proc. Sixth Int. Heat Transfer Conf.*, **1**, Toronto, Canada, pp. 157–161.
[12] Ward, H. C., 1982, ''Profile Description,'' in *Rough Surfaces* T. R. Thomas, ed., Longman Group, New York, pp. 72–90.
[13] Thomas, T. R., 1982, ''Stylus Instruments,'' in *Rough Surfaces* T. R. Thomas, ed., Longman Group, New York, pp. 12–70.
[14] Brown, W. T., Jr., 1967, ''Study of Flow Surface Boiling,'' Ph.D. thesis, M.I.T., Cambridge, MA.
[15] Mikic, B. B., and Rohsenow, W. M., 1969, ''A New Correlation of Pool-Boiling Data Including the Effect of Heating Surface Characteristics,'' ASME J. Heat Transfer, **91**, pp. 245–250.
[16] Bier, K., Gorenflo, D., Salem, M., and Tanes, Y., 1978, ''Pool Boiling Heat Transfer and Size of Active Nucleation Centers for Horizontal Plates With Different Surface Roughness,'' *Proc. Sixth Int. Heat Trans. Conf.*, **1**, Toronto, Canada, pp. 151–156.
[17] Yang, S. R., and Kim, R. H., 1988, ''A Mathematical Model of the Pool Boiling Nucleation Site Density in Terms of the Surface Characteristics,'' Int. J. Heat Mass Transf., **31**, pp. 1127–1135.
[18] Wang, C. H., and Dhir, V. K., 1993, ''Effect of Surface Wettability on Active Nucleation Site Density During Pool Boiling of Water on a Vertical Surface,'' ASME J. Heat Transfer, **115**, pp. 659–669.
[19] Gaertner, R. F., 1963, ''Distribution of Active Sites in the Nucleate Boiling of Liquids,'' Chem. Eng. Prog., Symp. Ser., **59**, pp. 52–61.
[20] Eckert, E. R. G., and Drake, R. M., 1972, *Analysis of Heat and Mass Transfer*, McGraw-Hill, New York.
[21] Panton, R. L., 1984, *Incompressible Flow*, John Wiley & Sons, New York.
[22] Mikic, B. B., Rohsenow, W. M., and Griffith, P., 1970, ''On Bubble Growth Rates,'' Int. J. Heat Mass Transf., **13**, pp. 657–666.
[23] Van Stralen, S. J. D., Sohal, M. S., Cole, R., and Sluyter, W. M., 1975, ''Bubble Growth Rates in Pure and Binary Systems: Combined Effect of Relaxation and Evaporation Microlayers,'' Int. J. Heat Mass Transf., **18**, pp. 453–467.
[24] Lee, H. S., and Merte, H., 1996, ''Spherical Vapor Bubble Growth in Uniformly Superheated Liquids,'' Int. J. Heat Mass Transf., **39**, pp. 2427–2447.
[25] Bankoff, S. G., 1958, ''Entrapment of Gas in the Spreading of a Liquid over a Rough Surface,'' AIChE J., **4**, pp. 24–26.
[26] Bankoff, S. G., and Mikesell, R. D., 1959, ''Bubble Growth Rates in Highly Subcooled Nucleate Boiling,'' Chem. Eng. Prog., Symp. Ser., **55**, pp. 95–102.
[27] Carey, V. P., 1992, *Liquid-Vapor Phase-Change Phenomena: An Introduction to the Thermophysics of Vaporization and Condensation Processes in Heat Transfer Equipment*, Hemisphere, New York.
[28] Bernardin, J. D., Mudawar, I., Walsh, C. B., and Franses, E. I., 1997, ''Contact Angle Temperature Dependence for Water Droplets on Practical Aluminum Surfaces,'' Int. J. Heat Mass Transf., **40**, pp. 1017–1034.
[29] Skripov, V. P., 1974, *Metastable Liquids*, John Wiley & Sons, New York.
[30] Spiegler, P., Hopenfeld, J., Silberberg, M., Bumpus, Jr., C. F., and Norman, A., 1963, ''Onset of Stable Film Boiling and the Foam Limit,'' Int. J. Heat Mass Transf., **6**, pp. 987–994.